А С Т Р О Ф И З И К А

ТОМ 63 АВГУСТ, 2020 ВЫПУСК 3

EXPLORING THE ORIGIN OF MULTIWAVELENGTH EMISSION FROM HIGH-REDSHIFT BLAZAR B3 1343 + 451

N.SAHAKYAN[1,2], G.HARUTYUNYAN[1], D.ISRAYELYAN[1], M.KHACHATRYAN[1]

Received 20 February 2020
Accepted 24 June 2020

B3 1343 + 451 is a distant ($z = 2.534$) and bright flat-spectrum radio quasar observed in the γ -ray band. The results from the multiwavelength observations of B3 1343 + 451 with Fermi-LAT and Swift are reported. In the γ -ray band, strong flares were observed on 05 December 2011 and on 13 December 2009 when the flux increased up to $(8.78 \pm 0.83) \cdot 10^{-7}$ photon cm^{-2} s^{-1}. The hardest photon index $\Gamma = 1.73 \pm 0.24$ has been observed on MJD 58089 which is not common for flat-spectrum radio quasars. The analysis of Swift XRT data shows that in 2014 the X-ray flux of the source increased ~2 times as compared to 2009, but in both periods the X-ray emission is characterized by a hard photon index of $\Gamma_{\text{X-ray}} = 1.2 - 1.3$. During the γ -ray flares, the shortest flux halving timescale was ~2.34 days, implying the emission had been produced in a very compact region, $R \leq \delta ct/(1+z) = 3.43 \cdot 10^{16}$ cm (when $\delta = 20$). The spectral energy distribution of B3 1343 + 451 is modeled during the quiescent and flaring periods assuming a compact emitting region outside the BLR. It is found that the flares can be explained by only changing the bulk Lorentz factor of the emitting region without significant modification of the emitting electron parameters and luminosity of the jet.

Keywords: *B3 1343 + 451: γ -rays: X-rays: Blazars*

1. *Introduction*. Blazars are radio-loud active galactic nuclei (AGNs) the relativistic jets of which are inclined toward the observer, i.e. have a small angle (several degrees) to the line of sight [1]. Due to this small inclination angle and relativistic motion, the intensity of these sources is significantly boosted in the observer frame and is dominated by the non-thermal emission produced inside the jet [2]. Blazars are observed throughout the electromagnetic spectrum, from radio to High Energy (HE) γ -rays, exhibiting a double-peaked structure. The first peak is believed to be produced from the synchrotron emission of electrons within the jet while the nature of the second component is debatable. Within well-known leptonic scenarios, this component is attributed to inverse Compton (IC) scattering of low-energy photons. The origin of the photon field mostly depends on the type of the blazars: for BL Lacs which have weak or no emission lines the synchrotron photons can serve as targets for IC scattering [3-5], while the SEDs of Flat Spectrum Radio Quasars (FSRQs) with stronger and quasar-like emission lines are better explained when the photons external to the jet are considered [6,7]. Alternatively, in hadronic scenarios the HE component is due to relativistic protons

accelerated within the jet, either via their synchrotron radiation [8], or via secondary emission from particles generated in the interaction of the protons with low-energy photon fields [9,10]. Now, these hadronic models are more frequently applied to model the multimessenger data from the observations of blazars after the association of neutrinos [11,12] with the TXS 0506+056 [13-16].

One of the most distinct characteristics of blazar emission is rapid and high amplitude variability across the whole electromagnetic spectrum. The most dramatic and short time scale changes have been observed in the γ-ray band. For example, Brown [17] showed that during the γ-ray flares of PKS 1510-089 the flux doubling timescale was as short as 1.3 ± 0.12 hr or Ackermann et al. [18] showed that the flux doubling time of 3C 279 2015 June flare was less than 5 minutes. Interestingly, in the γ-ray band, the emission from NGC 1275 radio galaxy is also variable in short time scales, 1.21 ± 0.22 hr, which had never been previously observed for any radio galaxy [19,20]. This strongly constrains the emitting region size, suggesting the radiation comes from the sub-parsec scale regions of the jet. Therefore the observations of blazars contain valuable information on the initial sub-parsec-scale region of their jets.

The distant blazar B3 $1343+451$ is among the FSRQs detected by Fermi-Large Area Telescope (LAT). During the recent years, it was reported [21,22] that several times this source was in the high emission/bright flaring state in the γ-ray band which is interesting considering the distance of B3 $1343+451$ ($z = 2.534$). Also, the source was monitored by the Neil Gehrels Swift observatory (Swift) several times in various years, providing the data in optical/UV and X-ray bands. Combining this with a large amount of data available in the γ-ray band (more than ten years) will allow a detailed investigation of the origin of multiwavelength emission from B3 $1343+451$. Moreover, for some periods the source was in a flaring state which allows to constrain the emitting region size and location, magnetic field, electron energy distribution, and so on which makes B3 $1343+451$ an ideal object for exploring the physics of the jets of distant FSRQs.

Here the broadband emission from B3 $1343+451$ is studied by analyzing Swift UVOT/XRT and Fermi-LAT data. The data analysis and reduction are presented in Section 2. The broadband SED modeling is presented in Section 3, and results and discussion are provided in Section 4. The conclusion is summarized in Section 5.

2. *Data analysis*. The data accumulated in the HE γ-ray band by Fermi-LAT is crucial for understanding the nature of variable emission from the blazars. The γ-ray data, being continuously accumulated since 2008, allows to indentify different emission states of the sources, compare them with the observations in the other bands and build contemporaneous SEDs necessary for the theoretical modeling. In order to investigate the origin of the emission from B3 $1343+451$,

initially the available γ-ray data have been analyzed.

2.1. *Fermi-LAT data extraction and analyses*. Fermi-LAT on board the Fermi satellite is a pair-conversion telescope, operating since August 4, 2008, and is designed to detect HE γ-rays in the energy range from 20 MeV to 300 GeV [23]. In this study, the data set collected during the first ten years of Fermi-LAT operation, from August 4, 2008, to August 4, 2018 (MET 239557417-555033605) was used. The data were analyzed with the standard Fermi Science Tools 1.2.1 software package using the most recent reprocessed PASS eight events and spacecraft data in the energy range from 100 MeV to 500GeV and using P8R3_SOURCE_V2 instrument response function. The entire data set is filtered with *gtselect* and *gtmktime* tools and only the events with a high probability of being photons *evclass* = 128, *evtype* = 3 have been considered. The zenith angle cutoff is made to exclude atmospheric γ-rays from the Earth limb that can be a significant source of background.

The photons from a circular region with a radius of 12° around the γ-ray position of B3 1343 + 451 (RA, Dec) =(206.394, 44.884) have been extracted. These photons are then binned with the *gtbin* tool with a stereographic projection into pixels of $0^{\circ}.1\times0^{\circ}.1$ and into 37 equal logarithmically-spaced energy bins. The model for which the likelihood is calculated is a combination of point-like sources within a $16^{\circ}.5\times16^{\circ}.5$ square region of interest (ROI) and diffuse Galactic and extragalactic models which were modeled using the standard *gll_iem_v06* and *iso_P8R2_SOURCE_V6_v06 models*. The model file describing ROI was created using the Fermi-LAT fourth source catalog (4FGL; [24]) which contains sources within ROI +5° from B3 1343 + 451. The normalization of background models, as well as fluxes and spectral indexes of the sources within the ROI, are considered as free parameters during the analysis, while for the sources outside the ROI the spectral slopes and normalizations were fixed to the values given in the 4FGL catalog.

Initially, for the whole time period, the binned likelihood analysis is performed by *gtlike tool* modeling the γ-ray spectrum of B3 1343 + 451 using a log-parabola [25] as in 4FGL. After constraining the parameters of all sources included in the model, the analysis is repeated assuming a power-law shape for the γ-ray spectrum of B3 1343 + 451. The output model is used in the light-curve calculations, as for the short periods the power-law model better represents the spectrum. The γ-ray light curves were calculated by repeating the same analysis for shorter time periods applying an unbinned maximum likelihood analysis method considering photons from 0.1 to 300 GeV energy range. In the model file obtained from the whole-time analysis, the photon indexes of all background sources are fixed to the best guess values in order to reduce the uncertainties in the flux estimations, but the normalization of sources within the ROI are free to vary. Since no variability is expected for the underlying background diffuse emission, we fixed their parameters to the average values obtained in the ten-year analysis.

The γ-ray light curve of B3 1343+451 computed for three-day bins above 100 MeV is shown in Fig.1. Several bright γ-ray emission states of the source can be identified, namely from MJD 55083 to 55116, from 55839 to 55965, from 56160 to 56235 and from 57021 to 57126. Interestingly, during the prolonged γ-ray active period from MJD 55720 to 57230, not only two major flares from the source were observed but also the flux increased from its average level and remained so for nearly 500 days. The peak flux of $(8.78 \pm 0.83) \cdot 10^{-7}$ photon cm^{-2} s^{-1} with a photon index of $\Gamma = 2.02 \pm 0.07$ was observed on MJD 56175 within three days with a detection significance of 25.1σ. Another substantial increase of the γ-ray flux has been observed on MJD 55893 when the flux was $(8.73 \pm 0.85) \cdot 10^{-7}$ photon cm^{-2} s^{-1} with $\Gamma = 2.10 \pm 0.08$ photon index and with 24.0σ detection significance. The γ-ray photon index variation in time computed for three-day bins is shown in the middle panel of Fig.1. Most of the time, the photon index varies around its averaged value reported in 4FGL (2.14 from the log-parabolic fit), but in some periods hardening and softening are evident. The hardest photon index of $\Gamma = 1.73 \pm 0.24$ has been observed on MJD 58089 with 6.2σ while the softest one 3.13 ± 0.31 was observed on MJD 57675. Unfortunately, in some periods the uncertainties

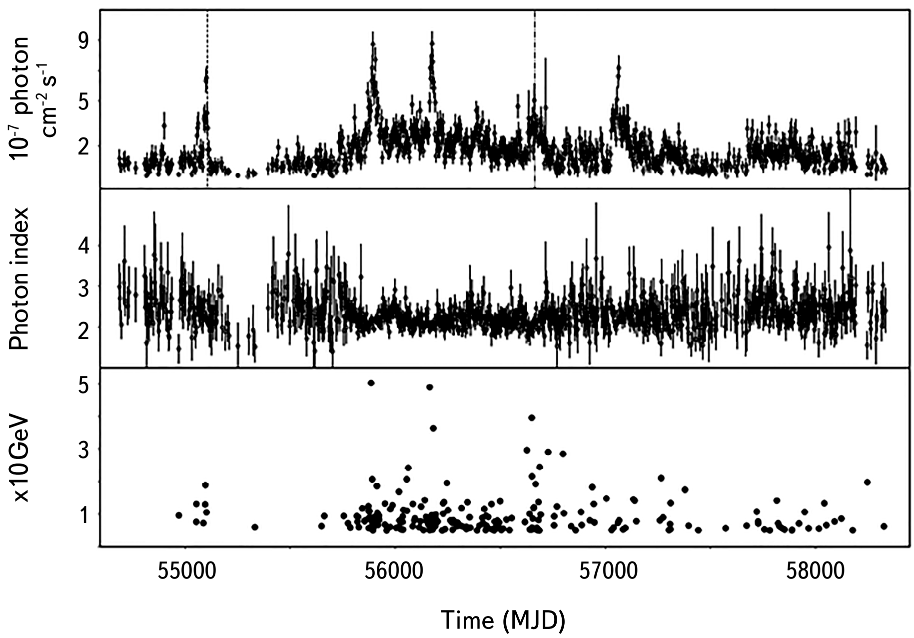

Fig.1. The evolution of γ-ray flux and spectral index of B3 1343 + 451 in time computed using 3-day bins. The lower panel shows the arrival time of HE photons (with energy >5 GeV).

in the photon index estimation are relatively large, which does not allow to make a definite conclusion on the variability of the spectral index.

The evolution of the γ-ray photon index was further investigated by plotting it versus flux (Fig.2a) considering only the time bins when the detection significance was above 4.0σ. From the plot, the averaged photon index and flux are $\sim 2\cdot 10^{-7}$ photon cm^{-2} s^{-1} and ~2.1, respectively. There is a hint of spectral hardening as the source gets brighter, i.e., during the bright periods the photon index of the source is relatively harder. In the γ-ray band such behavior has already been observed from several blazars (e.g., [26-28]) and radio galaxies (e.g., NGC 1275 [19]). Such evolution of the spectral index and flux is expected when accelerated HE electrons are cooled down (e.g., [29]). However, the linear-Pearson correlation test yields to $r_p = 0.05$ with *p*-value being 0.19. This implies there is a marginal linear correlation between the flux and photon index but it is not statistically significant.

During the three outbursts in the γ-ray band (the first three peaks in Fig.1

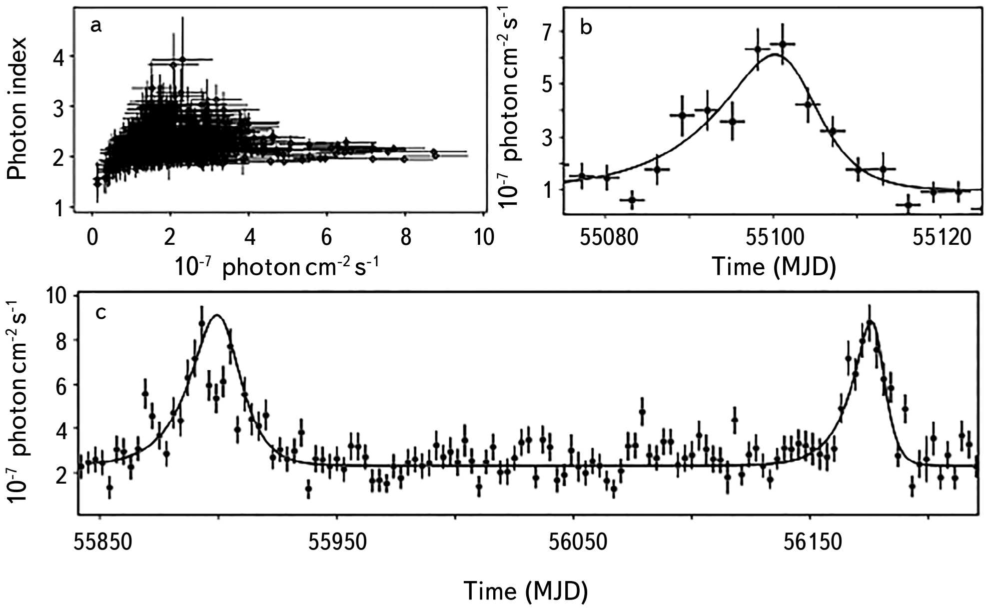

Fig.2. Upper left: B3 1343 + 451 γ-ray photon index vs. flux in three-day bins. Upper right and lower panels: the flare time profile analyses.

upper panel) the rising and decaying shapes of the flares can be well constrained by the data. The temporal evolution of each flare has been studied separately. For this purpose, we performed a time profile fitting of these flares by a sum of exponentials which gives the rise and decay times of each peak [30],

$$F(t) = F_c + F_0\left(\exp\frac{t_0 - t}{t_r} + \exp\frac{t - t_0}{t_d}\right)^{-1}$$

where F_0 is the flux at t_0 representing the approximate flare amplitude, F_c is the quiescent flux, t_r and t_d are the rise and decay times of the flare, respectively. The light curve was fitted with the nonlinear optimization python package *lmfit*[1].

The fitting parameters are summarized in Table 1 and the corresponding fit is shown in Fig.2b, c. The time profiles show asymmetric structures in all flares, showing a slow rise and a fast decay trend. The rise time of the first flare is 7.91 ± 1.84 days dropping within 3.38 ± 0.84 days. The time peak of the first flare, $t_p = t_0 + t_r t_d \ln(t_d/t_r)/(t_r + t_d)$ is at MJD 55100.3 with a flare amplitude of $(9.42 \pm 1.21)\cdot 10^{-7}$ photon cm^{-2} s^{-1}. The next flares are fitted together with the same constant level of the flux to reduce the number of free parameters. These flares reach the peaks within 11.34±2.85 and 9.21±2.43 days, respectively, then the second one quickly drops to its average level within 3.64±1.24 days while the decay of the other flare is relatively slow, 7.66±2.19 (Table 1). The time peak of the flares are at MJD 55899.5 and MJD 56175.98 with amplitudes of $(13.41 \pm 2.67)\cdot 10^{-7}$ and $(11.85 \pm 2.00)\cdot 10^{-7}$ photon cm^{-2} s^{-1}, respectively. The shortest flux doubling or halving timescales, computed by $t_{r,d} \ln 2$, is ~2.34 days.

Table 1

PARAMETER VALUES BEST EXPLAINING THE FLARES

t_m MJD	$t_r \pm err$ days	$t_d \pm err$ days	F_c x10^{-7} photon cm^{-2} s^{-1}	F_0 x10^{-7} photon cm^{-2} s^{-1}
55102.3 ± 1.59	7.91 ± 1.84	3.38 ± 0.84	0.99 ± 0.18	9.42 ± 1.21
55901.3 ± 3.97	11.34 ± 2.85	7.66 ± 2.19	2.31 ± 0.08	13.41 ± 2.67
56178.3 ± 2.32	9.21 ± 2.43	3.64 ± 1.24	2.31 ± 0.08	11.85 ± 2.00

The arrival time of the highest-energy events (>5 GeV) from the direction of B3 1343 + 451, calculated using the *gtsrcprob* tool, is shown in the lower panel of Fig.1. The HE photons are mostly at MJD 55720 - 57230; the maximum 50.3 GeV is at MJD 55884 with a 2.6σ probability is associated with B3 1343 + 451.

2.2. *Swift XRT/UVOT data analyses*. B3 1343 + 451 was observed three times by Swift, in 2009 and in 2014. The data from two of the instruments onboard Swift, the UltraViolet and Optical Telescope (UVOT) and from the X-Ray Telescope (XRT), have been analyzed. The Swift-XRT observations were made in the photon counting mode and the source count rate was always below 0.5 counts s^{-1}, so no pile-up correction was necessary. The data were analyzed using the XRTDAS software

---

[1] *https://lmfit.github.io/lmfit-py/*

package distributed by HEASARC as part of the HEASoft package (v.6.25). The source spectrum region was defined as a circle with a radius of 20 pixels (47") at the center of the source, while the background region was defined as an annulus centered at the source with its inner and outer radii being 51 (120") and 85 pixels (200"), respectively. The Cash statistics [31] on ungrouped data was used; the individual spectra in the 0.3-10.0 keV range were fitted with XSPEC v12.10.1, adopting an absorbed power-law model with $N_H = 1.78 \cdot 10^{20}$ cm^{-2} column density. Unfortunately, the number of counts in the single observations was relatively low, ~30 not allowing to estimate the parameters with a statistical significance. For example, for Obsid 38469006, the X-ray photon index and flux have been estimated to be 1.43±0.27 and $(6.57 \pm 2.41) \cdot 10^{-13}$ erg cm^{-2} s^{-1}, respectively. In order to increase the photon statistics, three sequential observations made in January 2014 (Obsid 38469004, 38469005 and 38469006) as well as two sequential observations made in October 2009 (Obsid 38469002 and 38469003) were merged to obtain the averaged X-ray spectra of the source in two different years. As a result, the X-ray photon index was 1.35±0.29 in 2009 and 1.20±0.21 in 2014. Similarly, the fluxes in 2009 and 2014 were $(4.06 \pm 1.19) \cdot 10^{-13}$ erg cm^{-2} s^{-1} and $(7.54 \pm 1.64) \cdot 10^{-13}$ erg cm^{-2} s^{-1}, respectively. Even if the photon index did not change significantly, taking into account the uncertainties, there had been a slight increase in the X-ray flux in 2014.

In the analysis of the Swift UVOT data, the source counts were extracted from an aperture of 5".0 radius around the source while the background counts were taken from the neighboring circular region having a radius of 20" and not being contaminated by nearby sources. The magnitudes were computed using the *uvotsource* tool (HEASOFT v6.25) then corrected [32] using the reddening coefficient from the Infrared Science Archive[2]. Like the XRT data analyses, the sequential observations made in 2009 and 2014 were merged to reduce the flux estimation uncertainties. The optical/UV flux derived in these two periods is shown in Fig.4.

2.3. *Spectral Analyses*. For the spectral analyses the data from the following periods are considered:

Low state: MJD 55125-55722, when the source was not flaring in the γ-ray and had a typical average flux.

Flare 1 (F1): MJD 55096.5-55102.5, corresponding to the highest peak of the flare on MJD 55100, coinciding with the Swift observations in 2009.

Flare 2 (F2) and Flare 3 (F3): 3 days period centered on MJD 55893 and on MJD 56175, corresponding to bright γ-ray states.

Flare 4 (F4): MJD 56629.5-56707.5, corresponding to another flaring γ-ray

[2] *https://irsa.ipac.caltech.edu/applications/DUST/*

state with available quasi-simultaneous Swift observation in 2014.

The spectrum of B3 1343 + 451 was modeled with a power-law function ($dN/dE \sim N_0 E^{-\alpha}$) with the normalization N_0 and index α as free parameters. The best matches between the spectral models and events are obtained with an unbinned likelihood analysis implemented in *gtlike*. Then, the SEDs are calculated by fixing the power-law index of B3 1343 + 451 and running *gtlike* separately for smaller energy bins of equal width in the log scale. The corresponding spectra are shown in Fig.3 (except for F3 when the spectrum is similar to that of F2) and the results of analyses are given in Table 2.

The γ -ray spectrum in all periods extends up to ~10 GeV (for F4 up to ~60 GeV). The photon index is soft during the low state, $\Gamma_\gamma = 2.46 \pm 0.05$, which hardens during the flaring periods. The hardest photon index of $\Gamma_\gamma = 2.00 \pm 0.04$ was observed during F3. During the F1, F2 and F3 flares, the source had a high flux of $(8.0 \pm 9.0) \cdot 10^{-7}$ photon $cm^{-2} s^{-1}$ which drops to $(2.79 \pm 0.12) \cdot 10^{-7}$ photon $cm^{-2} s^{-1}$ during F4. The flux at the

Table 2

FERMI-LAT SPECTRAL ANALYSES RESULTS

Period	Flux[a]	Γ_γ	σ
low	0.44±0.03	2.46±0.05	25.0
F1	6.39±0.57	2.22±0.08	23.5
F2	9.04±0.63	2.12±0.06	23.5
F3	8.68±0.50	2.00±0.04	23.8
F4	2.79±0.12	2.08±0.03	50.8

Notes: [a] γ -ray in units of x10^{-7} photon $cm^{-2} s^{-1}$.

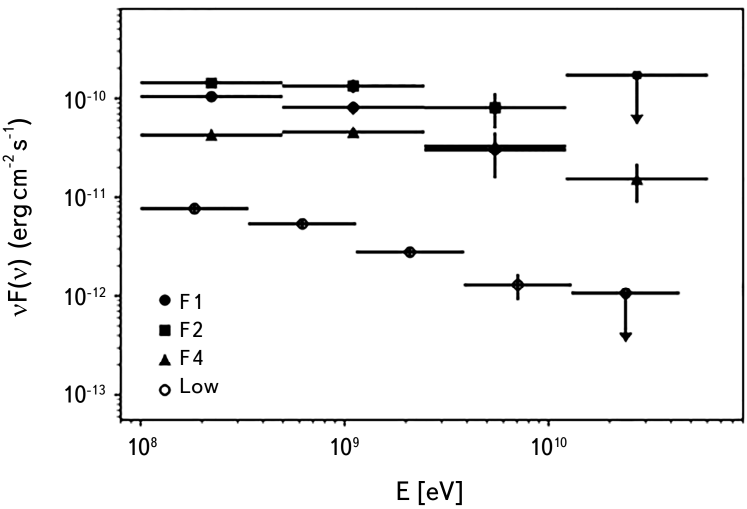

Fig.3. The γ -ray spectra of B3 1343 + 451 for flaring (F1, F2 and F4) and low states.

low state is ~20 times lower and corresponding to the baseline flux of the source emission in the γ-ray band.

3. *Modeling the SED*. The SED of B3 $1343+451$ during the quiescent (low), and flaring (F1 and F4) periods are shown in Fig.4. The γ-ray data are shown with black circles while for the F1 and F4 flares, the available optical/UV and X-ray data analyzed in Section 2 are shown with black triangles and squares, respectively. The data of F1 are shown with empty marks. The archival data from the ASI science data center are shown in gray. The broadband SED of B3 $1343+451$ shows a typical double-peaked structure: a low energy component, peaking in the optical through X-rays, originates from synchrotron emission of electrons and a high energy component, peaking in the γ-ray, probably originating from Compton scattering of the seed photon field, either internal (synchrotron self-Compton [SSC] [3-5]) or external to the jet (external Compton [EIC] [6,7]). In all periods the ratio of the IC to synchrotron luminosity is larger than one. In the Thomson regime, this ratio approximately corresponds to $L_{IC}/L_S \sim U_{photon}/U_B$ where U_{photon} and U_B are the energy density of the photon and magnetic fields, respectively. $U_{photon} > U_B$ condition is satisfied when the density of the external photons exceeds (photons from broad-line region (BLR) or dusty torus) the density of synchrotron photons, so the HE component is entirely described by EIC scattering. It should be noted that SSC and SSC+EIC mechanisms were also successful in explaining the multiwavelength emission from radio galaxies [33-35]. Since the previous studies of bright FSRQs showed that the regions outside the BLR are more favorable for the γ-ray emission [28,36], in this study we assume that the dissipation region of the jet R_{diss} is outside the BLR and infrared emission from dusty torus is the dominant external photon field. The SED of B3 $1343+451$ is modeled within the commonly applied one-zone emission scenario which assumes the broadband spectrum is produced from a single region of the jet during its propagation. Unlike the two-zone models, when the acceleration and emission of particles occur in different regions, in this case the accelerated electrons are cooling by synchrotron and IC emission in a compact spherical region of the jet (with a radius of R) which moves with relativistic velocities $\Gamma_{\rm jet}$. Thus, the emission will be boosted by $\delta = \Gamma_{\rm jet}(1-\beta\cos\theta)^{-1}$ ($\delta = \Gamma$ for small θ), and will appear brighter for the observer. The analyses of a large sample of γ-ray emitting FSRQs show that bright blazars have a mean bulk Lorentz factor of $\Gamma > 15$ [37], so for B3 $1343+451$ we assume $\delta = 20$. The radius of the emitting region can be inferred from the observed flux doubling timescale of ~2.34 days from the $R \le \delta ct/(1+z) = 3.43 \cdot 10^{16}$ cm relation. This region carries a magnetic field with an intensity of B and a population of relativistic electrons for which a power-law with exponential energy distribution, $N_e(\gamma_e) \sim (\gamma_e)^{-p} \exp[-\gamma_e/\gamma_{cut}]$ within γ_{min} and

γ_{max}, is assumed. This electron spectrum is naturally formed within the first-order Fermi acceleration (diffuse shock acceleration [38,39]), under dominant radiative cooling and/or a decreasing chance for HE particles to cross the shock front a large number of times. The EIC scattering of external photons is taken into account assuming that the IR radiation from the dusty torus which has a blackbody spectrum with a luminosity that scales with the disc luminosity as $\eta\, L_{disc}$ ($\eta = 0.6$ [40]) and fills a volume that for simplicity is approximated as a spherical shell with a radius of $R_{IR} = 2.5 \cdot 10^{18} \left(L_{disc} / 10^{45} \right)$ cm [40]. The disc luminosity is $L_{disc} = 5.38 \cdot 10^{45}$ erg s^{-1}, estimated by fitting the blue-bump seen in the data (Fig.4) which is the accretion disc emission component. The parameters best describing the data are estimated *through minuit* optimization[3] [41-43].

3.1. *The SED in quiescent state*. Initially, the SED in the quiescent state is modeled (Fig.4 upper panel) to estimate the baseline energy of the jet as well as the radiating particle energy distributions. The model parameters are

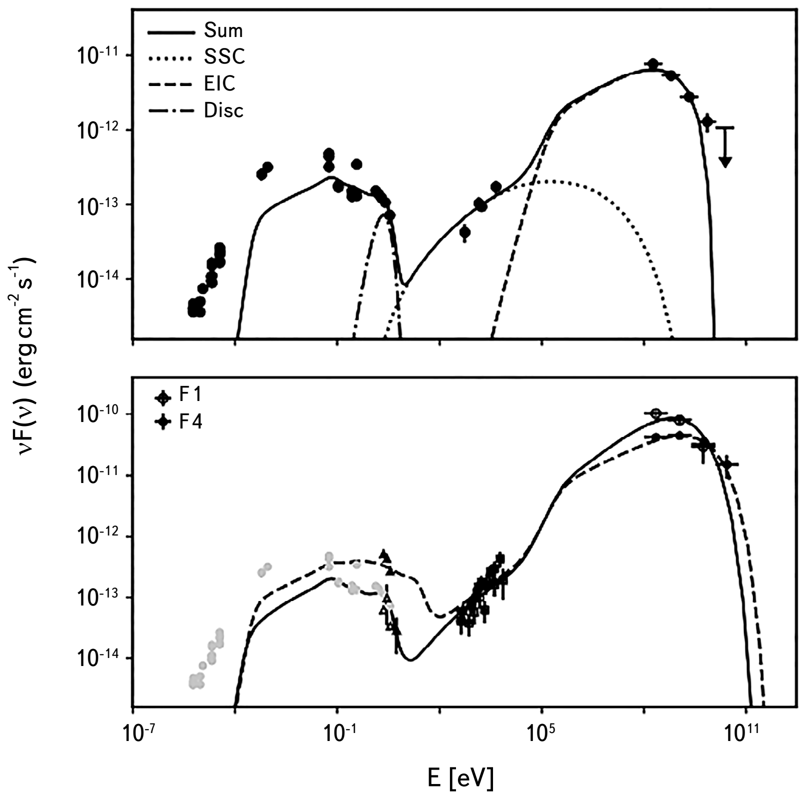

Fig.4. Modeling of the broadband SEDs of B3 1343 + 451 during the quiescent (upper panel) and flaring states (F1 and F4 lower panel). The model parameters are given in Table 3.

[3] *https://jetset.readthedocs.io/en/latest/*

Table 3

PARAMETERS BEST DESCRIBING THE SEDs

	Quiescent	F1	F4
δ	20	30	30
p	2.39	2.08	2.38
γ_{min}	62.78	62.78	62.78
γ_{cut}	4683.34	4884.00	12095.01
$B(G)$	0.18	0.04	0.10
U_e (erg cm^{-3})	0.10	0.13	0.09
U_B (erg cm^{-3})	$1.34 \cdot 10^{-3}$	$8.09 \cdot 10^{-5}$	$3.61 \cdot 10^{-4}$
L_e (erg s^{-1})	$1.12 \cdot 10^{45}$	$1.51 \cdot 10^{45}$	$1.04 \cdot 10^{45}$
L_B (erg s^{-1})	$1.49 \cdot 10^{43}$	$8.96 \cdot 10^{41}$	$4.00 \cdot 10^{42}$

given in Table 3. Since the radio emission is produced from the low-energy electrons which can diffuse larger distances, these data are not included in the fit and are considered as upper limits. In this case, the X-ray to γ-ray data is interpreted as IC up-scattering of synchrotron (dot-dashed line in Fig.4 upper panel) and torus (dashed line in Fig.4 upper panel) photons. The absence of high-quality X-ray data hardens the precise estimation of the power-law index of the electrons and $p = 2.39$ is defined by SSC fitting to X-ray data. When $\gamma_{min} = 62.78$, $\gamma_{cut} = 4683.34$ and $\gamma_{max} = 1.04 \cdot 10^4$, the EIC component peaks around GeV energies, explaining the γ-ray data. In the emitting region, the magnetic field is $B = 0.18$ G with a density lower than that of electrons $U_e/U_B = 74.6$ which implies that even if the system is not perfect in equipartition ($U_e/U_B = 1$), there is no large deviation between electron and magnetic field energy densities (for some blazars U_e/U_B can be as high as 1000).

3.2. *The SED in the flaring states.* The multiwavelength SEDs during the flaring states are shown in Fig.4 (lower panel). In the flaring states, the γ-ray flux significantly increased making the Compton dominance of the source stronger and evident. Such amplification of the emission spectra can be due to changes either in the emission region parameters, e.g., in the magnetic field, emitting region size, bulk Lorentz factor and others, and/or particle energy distribution. In principle, if the emission comes from a newly formed blob (e.g., ejected from the accretion disc) all the parameters describing the emitting region can be changed at the same time. To claim such global changes in the jet, sensitive radio observations are required which are missing in this case. The evolution of multiwavelength emission spectra in dependence with various parameters is performed in Paggi et al. [44]. Their Fig.1e shows that large magnitude variations are possible in the γ-ray band when the bulk Lorentz factor of the emission region increases. This is evident especially in the case of EIC scenario, since the density of external photons in the comoving frame of the jet depends on the Doppler boosting factor δ^2. Thus, in order to model the SEDs observed during the flaring periods, we assume that the Doppler boosting factor has increased and corresponds to $\delta = 30$.

During the fit, all the parameters describing the source (e.g., the luminosity of the torus, its radius, temperature, etc.) are fixed to the values obtained during the fit of the averaged state, while the parameters of the magnetic field and emitting electrons are left free to vary. Also, γ_{min} was fixed since it is obtained by requiring the model does not overproduce the radio data which are the same in all cases. X-ray to γ-ray data are again interpreted by the sum of SSC and EIC components (for the clarity only the sum of these components is depicted in Fig.4 lower panel) and the X-ray spectra can be explained when $p = 2.08$ and $p = 2.38$ for the flares F1 and F4, respectively. As the γ-ray spectrum during F4 is characterized by a harder photon index which extends to higher energies, larger $\gamma_{cut} = 12095.01$ is estimated as compared with F1 ($\gamma_{cut} = 4884.00$). In order to account the increase on the γ-ray flux, a higher energy densities of electrons are estimated (see Table 3) which results in lower magnetic field (0.04 and 0.10 for F1 and F4, respectively) to keep the flux of the lower component at the same level since the synchrotron emission depends on the total energy of electrons and magnetic field. During the flaring states, the jet of B3 1343 + 451 becomes more particle dominated with $U_e/U_B > 900$, which is natural considering the ratio of IC to synchrotron luminosity increases.

3.3. *Jet energetics*. The jet power in the form of the magnetic field and electron kinetic energy is calculated by $L_B = \pi c R_b^2 \Gamma^2 U_B$ and $L_e = \pi c R_b^2 \Gamma^2 U_e$, respectively (presented in Table 3). The jet luminosity on the form of the magnetic field L_B decreases from $1.5 \cdot 10^{43}\,\mathrm{erg\,s^{-1}}$ to $9.0 \cdot 10^{41}\,\mathrm{erg\,s^{-1}}$ while L_e does not vary much, remaining around $1.5 \cdot 10^{43}\,\mathrm{erg\,s^{-1}}$. This is because at flaring states the energy distribution of electrons extends to larger energies, i.e., has a larger γ_{cut} and or harder p, implying the total energy is distributed in more electrons.

4. *Results and discussion*. The results from γ-ray observations of the distant blazar B3 1343 + 451 from 2008 to 2018 are presented. The source was alternatingly in its active state, showing several prominent γ-ray flares. Starting from MJD 55720, within 500 days, the source was in a very active state when also its averaged flux increased as compared with normal states. During this period also two bright flares were observed, when the peak flux measured within a 3-day interval was $(8.78 \pm 0.83) \cdot 10^{-7}\,\mathrm{photon\,cm^{-2}\,s^{-1}}$ with a photon index of $\Gamma = 2.02 \pm 0.07$ observed on MJD 56175. This corresponds to isotropic γ-ray luminosity of $L_\gamma = 5.63 \cdot 10^{49}\,\mathrm{erg\,s^{-1}}$ for the distance of B3 1343 + 451 (21.04 Gpc). This is of

the same order with the highest luminosity of FSRQs observed in the γ-ray band so far. There is no evident variability of the γ-ray photon index but a period when $\Gamma = 1.73 \pm 0.24$ was observed on MJD 58089, which is not common for FSRQs. Although hard photon indexes have been occasionally observed during rapid flaring events in FSRQs [45], they are usually characterized by >2.3 indexes. The hard emission spectrum is most likely related to the emission of new energetic particles that were either injected into the emitting region or re-accelerated. However, the linear-Pearson correlation test did not result in a statistically significant correlation or anti-correlation between the flux and photon index which would allow testing one of the theories.

During the bright γ-ray flares, the time profile analyses showed an asymmetric profile of the flares which can be explained assuming that the particles are accelerated during the rising phase of the flare (e.g., by shock acceleration) and cool down or escape from the emitting region during the decay phase. This is in agreement with the observed Compton dominance, implying the density of the external photons in the jet's comoving frame increased. The observed shortest flux halving timescale is ~2.34 days, implying the emission is produced from a very compact region of the jet.

The analyses of Swift XRT data contemporaneous with the γ-ray flares on 2009 and 2014 show that the X-ray flux increased on 2014, $(7.54 \pm 1.64) \cdot 10^{-13}\,\mathrm{erg\,cm^{-2}\,s^{-1}}$, as compared with that of 2009, but the photon index did not change significantly, being hard in both periods. The increase of the X-ray is related to the similar increase observed in the γ-ray band which is most likely due to changes in the acceleration and cooling of the electrons.

The SEDs observed during quiescent and flaring states are modeled within one-zone leptonic models assuming that the jet dissipation occurs outside the BLR and considering both synchrotron and external photons for the IC scattering. In all periods, the SSC component can explain the X-ray data but the data in optical/UV bands (at 10^{15} Hz) limits the emitting electron maximum energy, and the SSC component cannot reach the HE γ-ray band. Instead, the γ-ray data can be explained only by considering the IC scattering of dusty torus photons (EIC). In the quiescent state, the electrons should be effectively accelerated up to 2.39 GeV ($m_e c^2 \gamma_{cut}$) with the power-law index of 2.39 in order to explain the observed data, while during F4 it should be up to 6.18 GeV. This is because in this period the γ-ray spectrum with a hard spectrum extends to higher energies as well as in the optical/UV band the spectrum slightly increases and shifts to higher energies (see Fig.4 lower panel). In the quiescent state the jet of B3 1343 + 451 is not far from the equipartition with U_e/U_B=74.6, while during the flares it is required that $U_e/U_B \geq 900$. This is natural, considering that during the flares the IC to synchrotron luminosities ratio is $L_{IC}/L_S \approx 150$. The flares are interpreted to be due to the changes in the bulk Lorentz factor, i.e. the contribution comes from a blob that moves faster. In this interpretation, the SEDs can be reproduced not changing the source parameters (e.g. torus luminosity, radius, etc.) but only varying the magnetic field and emitting electron parameters. As a result, the total jet luminosity estimated in the quiescent and flaring states is almost of the same order, supporting the assumption that the flares were caused by the change in the velocity of the emitting region rather than from a new energetically dominant component.

5. *Conclusion*. The origin of multiwavelength emission from B3 1343+451 during the quiescent and flaring states is investigated. In the γ-ray band, the flux varies within ~2.34 days with a peak flux of $(8.78 \pm 0.83) \cdot 10^{-7}$ photon cm^{-2} s^{-1}. Also, the photon index hardens as compared to its average value during the bright γ-ray periods.

The modeling of the SED of B3 1343+451 in the quiescent state allowed to constrain the properties of the jet when it is in the average emission state. The SED observed during the flares can be reproduced by changing the bulk Lorentz factor of the emission region and slightly changing the energy distribution of the emitting electrons, the total luminosity of the jet being constant. This implies that the flares are most likely produced in a different region as compared to the average state which does not dominate energetically but contains more energetic electrons.

In this paper, two flaring periods of B3 1343+451 were modeled providing information on the properties of the source jet. Identification of flaring periods in other distant blazars and their theoretical modeling can help to understand the physics of distant blazar jets.

Acknowledgements. This work was supported by the RA MES State Committee of Science, in the frames of the research project No 18T-1C335. This work used resources from the ASNET cloud and the EGI infrastructure with the dedicated support of CESGA (Spain).

[1] ICRANet Armenia Marshall Baghramian Avenue 24a, 0019 Yerevan, Armenia, e-mail: narsahakyan@gmail.com
[2] ICRANet Piazza della Republica 10, 65122 Pescara, Italy

ИССЛЕДОВАНИЕ ПРОИСХОЖДЕНИЯ МНОГОВОЛНОВОГО ИЗЛУЧЕНИЯ БЛАЗАРА B3 1343 + 451 С ВЫСОКИМ КРАСНЫМ СМЕЩЕНИЕМ

Н.СААКЯН[1,2], Г.АРУТЮНЯН[1], Д.ИСРАЕЛЯН[1], М.ХАЧАТРЯН[1]

B3 1343+451 является ярким и дальним ($z = 2.534$) квазаром с плоским спектром, наблюдаемым в γ-диапазоне. Приведены результаты многоволновых наблюдений B3 1343+451 с Fermi-LAT и Swift. В γ-диапазоне сильные вспышки наблюдались 5 декабря 2011г. и 13 декабря 2009г., когда поток увеличился до $(8.78 \pm 0.83) \cdot 10^{-7}$ фотон см$^{-2}$ с$^{-1}$. Самый маленький фотонный индекс $\Gamma = 1.73 \pm 0.24$ (наблюдался 1 декабря 2017г., MJD 58089), что не характерно для квазаров с плоским спектром. Анализ данных Swift XRT показывает, что в 2014г. рентгеновский поток источника увеличился в ~2 раза по сравнению с 2009г., но в обоих периодах рентгеновское излучение характеризуется жестким фотонным индексом $\Gamma_{\text{X-ray}} = 1.2 - 1.3$. Во время γ-вспышек самый короткий период, за который поток увеличился вдвое, был ~2.34 дня, что означает, что излучение исходит из очень компактной области $R \le \delta ct/(1+z) = 3.43 \cdot 10^{16}$ см (когда $\delta = 20$). Спектральное распределение энергии B3 1343+451 моделировалась в периоды покоя и вспышки, предполагая что компактная область излучения находится за пределами области свечения широких спектральных линий. Установлено, что вспышки могут быть объяснены только изменением коэффициента Лоренца излучающей области без существенного изменения параметров излучающих электронов и светимости струи.

Ключевые слова: *B3 1343+451: гамма излучение: рентгеновское излучение: блазары*

REFERENCES

1. *C.M.Urry*, *P.Padovani*, Publ. Astron. Soc. Pacif., **107**, 803, 1995.
2. *G.Ghisellini*, Radiative Processes in High Energy Astrophysics (Berlin: Springer), 2013.
3. *L.Maraschi*, *G.Ghisellini*, *A.Celotti*, Astrophys. J., **397**, L5, 1992.
4. *S.Bloom*, *A.Marscher*, Astrophys. J., **461**, 657, 1996.
5. *G.Ghisellini*, *L.Maraschi*, *A.Treves*, Astron. Astrophys., **146**, 204, 1985.
6. *M.Sikora*, *M.Begelman*, *M.Rees*, Astrophys. J., **421**, 153, 1994.
7. *M.Biazejowski*, *M.Sikora*, *R.Moderski et al.*, Astrophys. J., **545**, 107, 2000.

8. *A.Mucke*, *R.Protheroe*, Astroparticle Physics, **15**, 121, 2001.
9. *K.Mannheim*, Astron. Astrophys., **269**, 67, 1993.
10. *A.Mucke*, *R.Protheroe*, *R.Engel et al.*, Astroparticle Physics, **18**, 593, 2003.
11. *M.Aartsen*, *M.Ackermann*, *J.Adams*, Science, **361**, 147, 2018.
12. *P.Padovani*, *P.Giommi*, *E.Resconi et al.*, Mon. Not. Roy. Astron. Soc., **480**, 192, 2018.
13. *S.Ansoldi*, *L.A.Antonelli*, *C.Arcaro et al.*, Astrophys. J., **863**, L10, 2018.
14. *M.Cerruti*, *A.Zech*, *C.Boisson et al.*, Mon. Not. Roy. Astron. Soc., **483**, L12, 2019.
15. *N.Sahakyan*, Astrophys. J., **866**, 109, 2018.
16. *N.Sahakyan*, Astron. Astrophys., **622**, A144, 2019.
17. *A.Brown*, Mon. Not. Roy. Astron. Soc., **431**, 824, 2013.
18. *M.Ackermann*, *R.Anantua*, *K.Asano et al.*, Astrophys. J. Lett., **824**, L20, 2016.
19. *V.Baghmanyan*, *S.Gasparyan*, *N.Sahakyan*, Astrophys. J., **848**, 111, 2017.
20. *N.Sahakyan*, *V.Baghmanyan*, *D.Zargaryan*, Astron. Astrophys., **614**, A6, 2018.
21. *R.Buehler*, The Astronomer's Telegram, No.2217, 2009.
22. *O.Roopesh*, *M.Dutka*, *E.Torresi*, The Astronomer's Telegram, No.3793, 2011.
23. *W.B.Atwood*, *A.A.Abdo*, *M.Ackermann et al.*, Astrophys. J., **697**, 1071, 2009.
24. Fermi-LAT collaboration, arXiv e-prints, arXiv:1902.10045, 2019.
25. *E.Massaro*, *M.Perri*, *P.Giommi et al.*, Astron. Astrophys., **413**, 489, 2004.
26. *A.Abdo*, *M.Ackermann*, *M.Ajello et al.*, Astrophys. J., **710**, 810, 2010.
27. *A.Abdo*, *M.Ackermann*, *M.Ajello et al.*, Astrophys. J., **721**, 1425, 2010.
28. *S.Gasparyan*, *N.Sahakyan*, *V.Baghmanyan et al.*, Astrophys. J., **863**, 114, 2018.
29. *J.G.Kirk*, *F.Riege*, *A.Mastichiadis*, Astron. Astrophys., **333**, 452, 1998.
30. *A.Abdo*, *M.Ackermann*, *M.Ajello et al.*, Astrophys. J., **699**, 31, 2009.
31. *W.Cash*, Astrophys. J., **228**, 939, 1979.
32. *T.Poole*, *A.Breeveld*, *M.Page et al.*, Mon. Not. Roy. Astron. Soc., **383**, 627, 2008.
33. *N.Sahakyan*, *D.Zargaryan*, *V.Baghmanyan*, Astron. Astrophys., **574**, A88, 2015.
34. *D.Zargaryan*, *S.Gasparyan*, *V.Baghmanyan et al.*, Astron. Astrophys., **608**, A37, 2017.
35. *A.Abdo*, *M.Ackermann*, *M.Ajello et al.*, Astrophys. J., **719**, 1433, 2010.
36. *N.Sahakyan*, *S.Gasparyan*, Mon. Not. Roy. Astron. Soc., **470**, 2861, 2017.
37. *G.Ghisellini*, *F.Tavecchio*, Mon. Not. Roy. Astron. Soc., **448**, 1060, 2015.
38. *E.Summerlin*, *M.Baring*, Astrophys. J., **745**, 63, 2012.
39. *D.Ellison*, *F.Jones*, *S.Reynolds*, Astrophys. J., **360**, 702, 1990.
40. *G.Ghisellini*, *L.Maraschi*, *F.Tavecchio*, Mon. Not. Roy. Astron. Soc., **396**, L105, 2009.
41. *E.Massaro*, *A.Tramacere*, *M.Perri et al.*, Astron. Astrophys., **448**, 861, 2006.
42. *A.Tramacere*, *P.Giommi*, *M.Perri et al.*, Astron. Astrophys., **501**, 879, 2009.
43. *A.Tramacere*, *E.Massaro*, *A.Taylor*, Astrophys. J., **739**, 66, 2011.
44. *A.Paggi*, *A.Cavaliere*, *V.Vittorini et al.*, Astrophys. J., **736**, 128, 2011.
45. *L.Pacciani*, *F.Tavecchio*, *I.Donnarumma et al.*, Astrophys. J., **790**, 45, 2014.